Atmospheric Research 203 (2018) 207–215

Contents lists available at ScienceDirect

Atmospheric Research

journal homepage: www.elsevier.com/locate/atmosres

PMF and PSCF based source apportionment of $PM_{2.5}$ at a regional background site in North China

Zheng Zong[a,b], Xiaoping Wang[b], Chongguo Tian[a,*], Yingjun Chen[c,*], Shanfei Fu[d], Lin Qu[e], Ling Ji[e], Jun Li[b], Gan Zhang[b]

[a] Key Laboratory of Coastal Environmental Processes and Ecological Remediation, Yantai Institute of Coastal Zone Research, Chinese Academy of Sciences, Yantai 264003, China
[b] State Key Laboratory of Organic Geochemistry, Guangzhou Institute of Geochemistry, Chinese Academy of Sciences, Guangzhou 510640, China
[c] Key Laboratory of Cities' Mitigation and Adaptation to Climate Change in Shanghai (CMA), College of Environmental Science and Engineering, Tongji University, Shanghai 200092, China
[d] School of Environmental and Civil Engineering, Jiangnan University, Wuxi, Jiangsu Province 214122, China
[e] Yantai Oceanic Environmental Monitoring Central Station, SOA, Yantai 264006, China

ARTICLE INFO

Keywords:
Source apportionment
$PM_{2.5}$
PMF
PSCF
Geographical origin

ABSTRACT

To apportion regional $PM_{2.5}$ (atmospheric particles with aerodynamic diameter < 2.5 μm) source types and their geographic pattern in North China, 120 daily $PM_{2.5}$ samples on Beihuangcheng Island (BH, a regional background site in North China) were collected from August 20th, 2014 to September 15th, 2015 showing one-year period. After the chemical analyses on carbonaceous species, water-soluble ions and inorganic elements, various approaches, such as Mann-Kendall test, chemical mass closure, ISORROPIA II model, Positive Matrix Factorization (PMF) linked with Potential Source Contribution Function (PSCF), were used to explore the $PM_{2.5}$ speciation, sources, and source regions. Consequently, distinct seasonal variations of $PM_{2.5}$ and its main species were found and could be explained by varying emission source characteristics. Based on PMF model, seven source factors for $PM_{2.5}$ were identified, which were coal combustion + biomass burning, vehicle emission, mineral dust, ship emission, sea salt, industry source, refined chrome industry with the contribution of 48.21%, 30.33%, 7.24%, 6.63%, 3.51%, 3.2%, and 0.88%, respectively. In addition, PSCF analysis using the daily contribution of each factor from PMF result suggested that Shandong peninsula and Hebei province were identified as the high potential region for coal combustion + biomass burning; Beijing-Tianjin-Hebei (BTH) region was the main source region for industry source; Bohai Sea and East China Sea were found to be of high source potential for ship emission; Geographical region located northwest of BH Island was possessed of high probability for sea salt; Mineral dust presumably came from the region of Mongolia; Refined chrome industry mostly came from Liaoning, Jilin province; The vehicle emission was primarily of BTH region origin, centring on metropolises, such as Beijing and Tianjin. These results provided precious implications for $PM_{2.5}$ control strategies in North China.

1. Introduction

Aerosols are airborne solid or liquid particles, which are emitted directly or result from gas-to-particle conversions from multiple natural and anthropogenic sources (Bressi et al. 2014). In recent years, fine particles < 2.5 μm in aerodynamic diameter ($PM_{2.5}$) becomes the primary air pollutant in China due to some combined effects, such as rapid industrialization, high population densities, and meteorological factors that lead to weak dilution and dispersion (Niu et al. 2016). Furthermore, it evolves to a top environmental issue because of its strong adverse effects on human health, visibility, weather and climate (Liu et al. 2014), which has triggered both public alarm and official concern. Based on the epidemiology and resulting guidance of international organization, national legislation in many countries has fixed thresholds, policies for controlling $PM_{2.5}$ mass concentration (Masiol et al. 2017). In China, the government promulgated the First Grade National Ambient Air Quality Standard of China (35 μg m^{-3} for $PM_{2.5}$, GB 3095-2012) and introduced the Action Plan for Air Pollution Prevention and Control (2013-17), which aimed at marked improvements in air quality until 2017. Although the political abatement has alleviated the polluted status, air pollution in China is still far from being controlled, especially in the heavily polluted area, such as the North

* Corresponding authors.
E-mail addresses: cgtian@yic.ac.cn (C. Tian), yjchentj@tongji.edu.cn (Y. Chen).

https://doi.org/10.1016/j.atmosres.2017.12.013
Received 6 November 2017; Received in revised form 19 December 2017; Accepted 28 December 2017
Available online 29 December 2017
0169-8095/

China. In 2016, the proportion of fine days with $PM_{2.5}$ concentration lower than 35 μg m^{-3} in this region was only 56.8%, 22.0% lower than the national average. Also, nine of the ten cities ranking at the bottom of 74 cities in China with the relative worse air quality were located in the area (http://www.zhb.gov.cn/). Therefore, the improvement of air quality in North China is the crux to achieve the national setting goal by 2017.

Source identification and quantification are the key points to reduce the concentration of $PM_{2.5}$. For this, various studies have been conducted targeting big cities in this region for establishing an efficient control strategy to improve air quality (Li et al., 2016; Wu et al. 2015). However, such research results seem to be rather insufficient for pollution control, which may be ascribed to the lack of the regional source information of $PM_{2.5}$ (Kotchenruther 2016). It is because the diffusion and transport of $PM_{2.5}$ could pose a huge challenge to the pollution control (S-H Wang et al. 2016b). Thus, regional scale efforts to assess source apportionment of ambient $PM_{2.5}$ should be addressed. Monitoring data from background area could be used to assess the sources, as they are beyond the influence of pointing source, and therefore, better suited for investigating the regional pollution. As an illustration, biomass burning and biogenic emission were found to be the predominant sources for aerosols in East China in summer and autumn based on an observation at a regional background site in Ningbo (Liu et al. 2013). In addition, the geographical origin of $PM_{2.5}$ in North China is also important, but poorly documented. To the best of our knowledge, few studies have addressed this issue in this region (Zhang et al. 2013). Thus, regional source apportionment of $PM_{2.5}$ including both source and geographical origin information is urgently needed. In the present study, year-round $PM_{2.5}$ samples were collected on Beihuangcheng (BH) Island, a regional background site in North China, for a better understanding of the source and geographical origin of $PM_{2.5}$. The objects of this study are (1) to qualify the regional scale concentration burden and characteristics of $PM_{2.5}$ and its species; (2) to assess the sources of $PM_{2.5}$ based on chemical mass closure method and Positive Matrix Factorization (PMF) model; (3) to distinguish the source region of $PM_{2.5}$ using Potential Source Contribution Function (PSCF) model linked with PMF model. This effort is vital, as it would help to facilitate effective control strategies to mitigate air pollution in North China.

2. Materials and methods

2.1. Sampling site and sample collection

The sampling campaign was conducted from August 20th, 2014 to September 15th, 2015 at the Environmental Monitoring Station of State Ocean Administration of China on BH Island (38°24′N, 120°55′E). The island lies at the demarcation line between Bohai Sea and Yellow Sea (Fig. 1), which is about 65 km north of Shandong peninsula, 185 km east of Beijing-Tianjin-Hebei (BTH) region, and 43 km south of Liaodong peninsula. There is no industry found on it, and the majority of islanders live by fishing and seafood farming. Influenced by the Asian monsoon, the arriving air masses covered over most area of North China (Fig. S1), showing prefect regional background features.

During the sampling period, a total of 120 $PM_{2.5}$ samples were collected every three day by a Tisch high volume sampler at a flow rate of 1.13 m^3 min^{-1}. Blank samples were also collected to subtract possible contamination occurring during or after sampling. The duration of every sampling was 24 h starting at 06:00 am (local time). The quartz fiber filters used were preheated at 450 °C for 6 h in muffle furnace to remove the impurity. Before and after each sampling, quartz fiber filters were subjected to 24 h equilibration at 25 ± 1 °C and 50 ± 2% relative humidity, then analyzed gravimetrically using a Sartorius MC5 electronic microbalance. Each sample was weighted at least three times, and acceptable difference among the repetitions was < 20 μg for a sampled filter and 10 μg for a blank filter. After weighting, filters were folded, wrapped in aluminium foil, sealed in airtight plastic bags, and then stored in refrigerators (− 20 °C) until chemical analysis.

2.2. Chemical analysis

Organic carbon (OC) and element carbon (EC) were analyzed by a Desert Research Institute (DRI) Model 2001 Carbon analyzer (Atmoslytic Inc., Calabasas, CA) based on the Interagency Monitoring of Protected Visual Environment (IMPROVE_A) thermal/optical reflected (TOR) protocol. Detailed information can be referred to our previous study (Zong et al. 2015). Regarding water-soluble ions (Na^+, K^+, Ca^{2+}, Mg^{2+}, NH_4^+, Cl^-, NO_3^- and SO_4^{2-}), they were measured by an ion chromatograph (Dionex ICS3000, Dionex Ltd., America) following the analysis method (Shahsavani et al. 2012) with the detection limit of 10 ng ml^{-1} (error < 5%). The concentrations of inorganic elements were determined by an inductively coupled plasma coupled with mass spectrometer (ICP-MS of ELAN DRC II type, Perkin Elmer Ltd., Hong Kong) based on previous analytical method (Wang et al. 2006). The detection limit was < 0.01 ng ml^{-1}, and error < 5%. Noted, all the analytical species were blank-corrected by subtracting the average field blank value.

2.3. Data analysis method

2.3.1. HYSPLIT model

The hybrid single-particle Lagrangian integrated trajectory (HYSPLIT) model is a complete system for computing simple air parcel trajectories to complex dispersion simulation (Zhang et al. 2014), which is available on the National Oceanic and Atmospheric Administration Air Resource Laboratory website (www.arl.noaa.gov/ready/hysplit4.html). In this study, it was used to generate 72 h backward trajectory with 6 h interval, and 480 backward trajectories in total were calculated at 500 m above ground level (half of mixing height in North China). The calculated trajectories were then bunched into clusters by the clustering function in this model.

2.3.2. PMF model

Positive Matrix Factorization (PMF) recommended by the USEPA was utilized to qualify $PM_{2.5}$ sources in present research. It is available at the website: www.epa.gov/air-research/positive-matrix-factorizationmodel-environmental-data-analyses. PMF does not require the source profiles prior to analysis and has no limitation on source number, which is an effective source apportionment receptor model and has been widely used in works about the source apportionment of $PM_{2.5}$ (Zhang et al. 2013). The principles of PMF can be referred to elsewhere in detail (Amil et al. 2016). For species uncertainty, if the concentration is less than or equal to the method detection limit (MDL) used, the uncertainty (Unc) is calculated using the following equation:

$$Unc = \frac{5}{6} \times MDL$$

If the concentration is greater than the MDL used, the uncertainty would be calculated based on the equation:

$$Unc = \sqrt{(\text{ErrorFraction} \times \text{concentration})^2 + (0.5 \times \text{MDL})^2}$$

In total, twenty-eight chemical components were used for the PMF model, which included OC, EC, Cl^-, SO_4^{2-}, NO_3^-, Na^+, K^+, Ca^{2+}, Mg^{2+}, NH_4^+, Ti, V, Cr, Mn, Fe, Co, Ni, Cu, Zn, As, Cd, La, Ce, Pr, Nd, Pb, Th, U. To determine the optimal number of source factors, a string of effective test, in which factors number was from four to ten, was carried out. The resulting Q parameters were shown in Fig. S2. Obviously, there was a lowest Q_{Robust} value (7338) at seven factors in moving from four to ten factors. Although $Q_{expected}$ has been decreasing in the process, $Q/Q_{expected}$ shared similar variation with Q_{Robust} showing the lowest value at seven factors. In addition, PMF was run many times

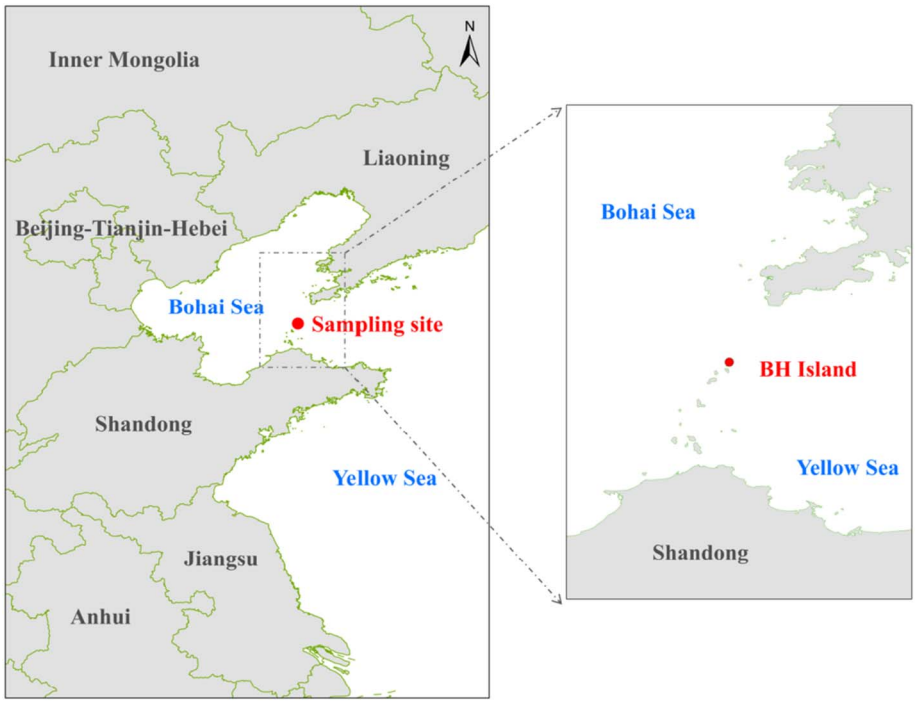

Fig. 1. Location of sampling site on BH Island.

with different F_{peak} to determine the range within which the objective Q_{Robust} remained relatively constant. Finally, an F_{peak} value (−0.1) at seven factors demonstrated the most physically reasonable source profiles. Uncertainty of PMF model is usually estimated by bootstrapping (BS), displacement (DISP), and bootstrapping with displacement (BS-DISP). Here, characteristics of factors nearby seven, where Q_{Robust} was relative lower, were explored. With six factors, four factors (coal combustion + biomass burning, ship emission, sea salt, vehicle emission) were mapped 100% of BS, while industry source and mineral dust were mapped 88% and 91%, respectively of runs. There were no swaps with DISP, and 100% of the BS-DISP runs were successfully. At seven factors, results were more stable with all factors but ship emission (mapped 96% of runs) mapped in BS in 100% (Table S1), no swaps occurred with DISP and all BS-DISP runs were successfully. However, the solution became less stable in moving from seven to eight factors. The new vehicle dust factor was only mapped in BS in 76% and ship emission factor was mapped in BS in 90%, other factors were mapped in 100% of runs. No swaps were found in DISP, but 24% of BS-DISP runs were rejected due to factor swaps. Therefore, it suggested that seven factors were the optimal solution in this study.

2.3.3. PSCF model

The Potential Source Contribution Function (PSCF) is an effective method to identify regional source on the basis of HYSPLIT model. In our study, it was adopted to assess the potential source regions of the indicative source factors from PMF result using the respective daily contribution data (Bressi et al. 2014). Briefly, the ij_{th} component of a PSCF field can be resumed as follows:

$$PSCF_{ij} = m_{ij}/n_{ij}$$

where n_{ij} is the total number of end points that fall in the ij_{th} cell, and m_{ij} is the number of endpoints of that parcel for which measured values exceed a user-determined threshold criterion (75th percentile chosen in this study). Noted, cells with few endpoints may result in high uncertainty in PSCF method. Thus, to remove these high uncertainties, an arbitrary weight function $W(n_{ij})$ was multiplied into the PSCF value:

$$W(n_{ij}) = \begin{cases} 1.00 & (n \geq 40) \\ 0.7 & (10 \leq n \leq 40) \\ 0.42 & (5 \leq n \leq 10) \\ 0.17 & (n \leq 5) \end{cases}$$

3. Results and discussion

3.1. General characteristics of $PM_{2.5}$ and its identified species

Table S2 shows a statistic summary of concentrations of $PM_{2.5}$, carbonaceous components, water-soluble ions (WSI) and inorganic elements on BH Island in the entire sampling period (annual and seasons). Generally, the concentration of $PM_{2.5}$ ranged from 5.28 μg m^{-3} to 267.11 μg m^{-3} with an annual mean of 63.10 ± 39.00 μg m^{-3}, which was about twice of the First Grade National Ambient Air Quality Standard (35 μg m^{-3}) of China (GB 3059-2012, www.zhb.gov.cn). Compared with other regions in China (Table S3), it was notably lower than those in typical urban areas, such as Beijing (135 μg m^{-3}), Chengdu (119 μg m^{-3}) and Guanzhong (134.7 μg m^{-3}), while was similar with some background sites. This indicated our measurement primarily reflected a regional pollution pattern, which was further confirmed by its seasonal back trajectory clusters (Fig. S1). A distinct seasonal variation of $PM_{2.5}$ was observed with the highest concentration (72.45 μg m^{-3}) in winter and the lowest value (45.84 μg m^{-3}) in summer. The concentration of $PM_{2.5}$ is usually governed by emission, meteorological condition and deposition process (Tao et al. 2014), thus the higher $PM_{2.5}$ concentration in winter could be partly attributed to the relative weaker atmospheric horizontal diffusion ability and vertical exchange capacity (Kumar et al. 2017). In addition, the wintertime residential coal combustion for heating in North China may be a great additional source for $PM_{2.5}$ (Huang et al. 2017). Except for OC, EC and SO_2, it was also the major source of nitrogen oxide (NO_x) in winter, significantly promoting the formation of new particle (Pan et al. 2016; G Wang et al. 2016a). By contrast, summer was possessed of favourable conditions for lower concentration, such as less emission and abundant rainfall (Lewandowski et al. 2007). On BH Island, the rainfall averaged

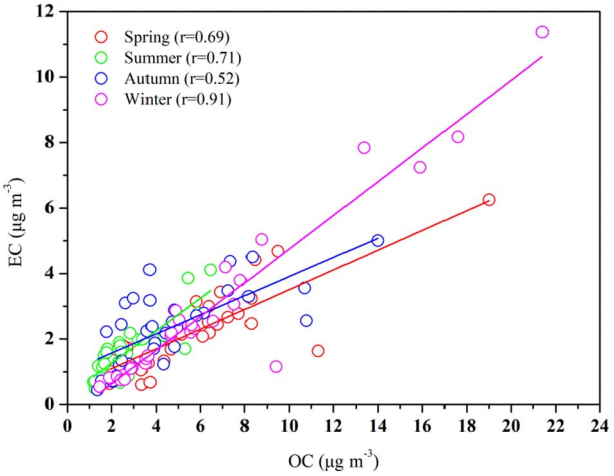

Fig. 2. Scatter plot showing the seasonal correlations between OC and EC in $PM_{2.5}$.

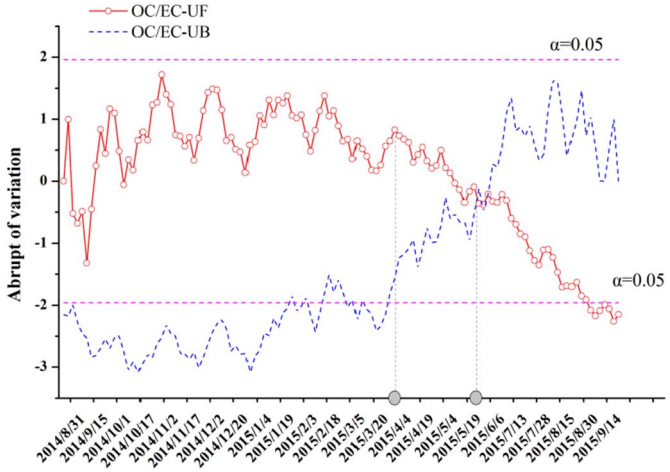

Fig. 3. Abrupt variation of OC/EC by M-K test on BH Island. Two pink dotted lines show the range of significant level at 95%. (For interpretation of the references to colour in this figure legend, the reader is referred to the web version of this article.)

153.52 mm in summer accounting for 66.96% of the total year, which accelerated the efficient removal of $PM_{2.5}$ from the atmosphere.

Carbonaceous species are important components in $PM_{2.5}$ (Feng et al. 2009). On BH Island, the average concentrations of OC and EC were 4.90 ± 3.69 and 2.28 ± 1.69 μg m^{-3}, respectively. Seasonally, the variations of OC and EC concentrations were both similar with that of $PM_{2.5}$ following the decreasing order of winter, autumn, spring and summer. The consistent variation of OC and EC may indicate their strong association of emission sources. For further understanding the relationship between OC and EC, the scatter plot was conducted as shown in Fig. 2. Obviously, OC and EC exhibited a good liner relation ($r > 0.52$, $p < 0.01$) during all the sampling time indicating their strong co-emission, especially in winter ($r = 0.91$). Generally, EC derives primarily from the incomplete combustion of carbon-contained materials, while OC includes primary organic carbon (POC) and secondary organic carbon (SOC) (Hu et al. 2014; Wang et al. 2014). The concentrations of SOC and POC were calculated by the EC tracer method:

$$SOC = OC - (OC/EC)_{prim} \times EC$$

$$POC = OC - SOC$$

where $(OC/EC)_{prim}$ is the ratio of OC/EC for primary emission. The minimum OC/EC was adopted as $(OC/EC)_{prim}$ (Du et al. 2014). The estimated concentrations of SOC and POC were 3.08 and 1.81 μg m^{-3}, respectively, with large seasonal discrepancies. The highest POC/OC (0.72) was found in winter followed by summer (0.66), spring (0.55) and autumn (0.45). It consisted with the order of correlation coefficient of OC and EC, also suggesting that the largest co-emission of OC and EC occurred in winter. Low-temperature burning, such as biomass burning, emits more OC compared with high-temperature burning (e.g. vehicle exhaust) (Gibson et al. 2013). Therefore the ratio of OC/EC could be used to evaluate the relative contribution of high- and low-temperature emission for OC and EC (Zong et al. 2016b). The ratio of OC/EC was 2.59, 1.80, 2.11 and 2.78 in spring, summer, autumn and winter, respectively. It suggested biomass burning contributed clearly to the carbonaceous species in winter on BH Island. Mann-Kendall (M-K) test could be adopted to test a non-liner trend and to determine the timing of each abrupt change for the time variation (Wang et al. 2014). In order to further identify the temporal tend of OC/EC, it was performed as shown in Fig. 3. Apparently, the abrupt point occurred at mid-May, exhibiting significant decrease at a 95% confidence interval level. But this decrease trend started as early as the end of March. It was an interesting phenomenon because the change point was in accordance with the time of stopping heating in North China. Thus coal combustion may be an important source for OC and EC in winter in North China.

For WSI, their concentrations averaged 25.99 ± 20.71 μg m^{-3}, which were 41.20% of $PM_{2.5}$ mass concentration. Among the ions, SO_4^{2-} ranked the highest with a mean value of 11.38 ± 10.26 μg m^{-3}, followed by NO_3^- (6.45 ± 4.92 μg m^{-3}) and NH_4^+ (4.91 ± 4.10 μg m^{-3}). The three secondary inorganic aerosols (SIA) constituted the majority (87.46%) of the total WSI, which was relative higher than urban areas agreeing with the regional scale of their precursors in North China (Zhao et al. 2012). It further suggested that our measurement provided a regional signal of $PM_{2.5}$ pollution in North China. By using ISORROPIA II model (Text S1), it can be seen SO_4^{2-} and NO_3^- were mostly combined with NH_4^+ presenting in the form of NH_4NO_3 and $(NH4)_2SO_4$, while the remainder SO_4^{2-} neutralized the alkalis, and all Cl^- was exclusively presented in the form of NH_4Cl (Table S4; Text S2). K^+ is usually treated as the marker of biomass burning (Fourtziou et al. 2017). Its concentration was relative higher in winter demonstrating the significance of biomass burning at that time, which consisted with the conclusion indicated by the higher ratio of OC/EC. Some typical ocean emission tracers, such as Na^+ and Mg^{2+}, exhibited the highest concentration in spring, which may be due to the mechanical disruption of the ocean surface under the higher wind speed. The ratio of Cl^-/Na^+ was highest in winter with the value of 3.03, followed by autumn (1.47), summer (1.47) and spring (1.26). Compared with seawater (Cl^-/Na^+, 1.80), the highest ratio in winter can be ascribed to the additional emission of Cl^- from coal combustion (Tian et al. 2016), while the lower values in other seasons may be due to the Cl^- deletion from reaction of nitric and sulfuric acid with NaCl particles and subsequent volatilization of HCl (Genga et al. 2017). In addition, the highest concentration of Ca^{2+}, the typical tracer of dust, was found in spring, corresponding to the prevalence of dust events at that moment (Huang et al. 2010).

Inorganic elements constitute a minor fraction of $PM_{2.5}$ mass. However, as primary pollutant, they are expected to conserve the finger-print of emission source for $PM_{2.5}$ (Tan et al. 2014). Total concentration of analyzed inorganic elements was 781.82 ± 670.96 ng m^{-3}, contributing 1.24% to the $PM_{2.5}$ mass. Its seasonal variability was not obvious. The lowest concentration was found in autumn, while values in spring, summer and winter were insignificant different (95%). Anthropogenic Zn (214.22 ± 196.80 ng m^{-3}) ranked the highest, followed by Fe (212.10 ± 267.48 ng m^{-3}) and Pb (151.13 ± 257.06 ng m^{-3}), implying the great contribution of human activities. In order to evaluate the contaminating degree, enrichment factors (EFs) method (Text S3) was employed as displayed in Fig. 4. Manifestly, the annual EFs of Ti, Yb, Lu, Tm, Er, Y, Ho, Th, Dy, Nd, Pr, Tb, Sm, Gd, Ce, Eu, U and La were lower than 10, indicating their main nature sources, while that of Co and Mn was slightly above 10, which respected a hybrid contribution from crustal and anthropogenic sources. The

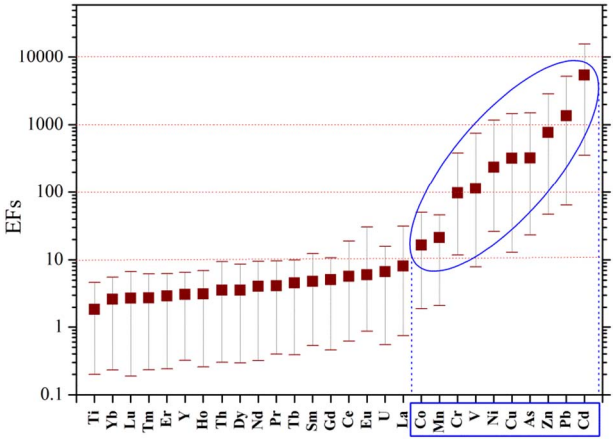

Fig. 4. EFs of inorganic elements in $PM_{2.5}$ on BH Island.

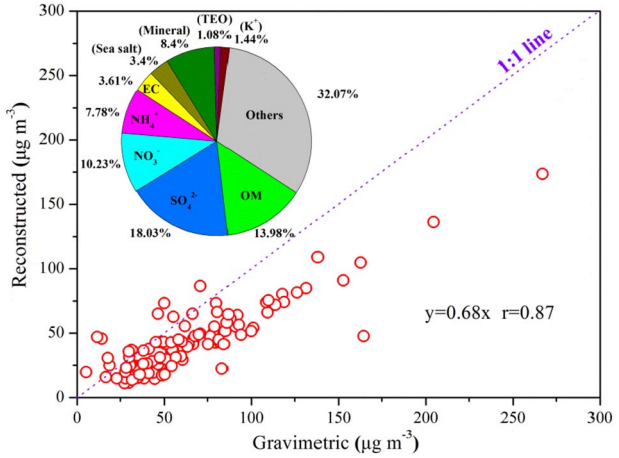

Fig. 5. The correlation between observed $PM_{2.5}$ and reconstructed $PM_{2.5}$ with the information of chemical mass closure on BH Island.

EFs of Cr, V, Ni, Cu, Zn, As, Cd and Pb were higher than 100, confirming their predominantly originations from human activities (Tao et al. 2014). Compared with other regions of China, such as Chengdu and Foshan, EFs of Ni and V (typical tracers of ship emission) on BH Island were much higher, revealing the ship emission for $PM_{2.5}$ in Bohai region (Zhang et al. 2014). This was further confirmed by the ratio of V/Ni (1.21 ± 0.5), much higher than the threshold value (0.7). For further identifying the contaminating characteristic of these anthropogenic elements (Co, Mn, Cr, V, Ni, Cu, As, Zn, Pb and Cd), the seasonal features of EFs were exhibited in Table 1. The highest EFs of V and Ni were found in summer indicating the biggest shipping contribution at that point. This agreed with previous study demonstrating shipping activities were more frequent in summer (Wang et al. 2013). Apart from V and Ni, Cu and As, Pb and Cd shared homogeneous seasonal fluctuation for EFs, which may suggest their co-emission in Bohai region.

3.2. Source apportionment of $PM_{2.5}$

3.2.1. Chemical mass closure

$PM_{2.5}$ mass was reconstructed on a seasonal and annual basis by employing chemical mass closure method (Text S4). On an annual scale, good correlation between observed and reconstructed $PM_{2.5}$ was found with an r of 0.87 (Fig. 5), suggesting a fine performance of the equation applied. The slope (0.68) was similar with that of Beijing (0.68) (Zhang et al. 2013), but lower than those in Chengdu (0.92) (Tao et al. 2014), Chongqing (0.80) (Yang et al. 2011) and Lanzhou (0.97) (Y Wang et al. 2016c). Correspondingly, the unidentified portion reached 32.07%. One reason for such high ratio of the unidentified was the lack of water content in this study as various studies have shown that water content was one of the important components in $PM_{2.5}$ mass. By using a KF system equipped with a controlled heating device, a recent study reported that the PM-bound water could constitute up to 22% of the total PM matter (Perrino et al. 2016). Another possible reason was the varying factors adopted for the transformation from measured species to certain components. For example, OM/OC ratio often ranges from 1.4 to 2.2, which was intended as 1.8 in present study. If we employed the factor of 2.2, the unidentified percentage would fall by 3.11%.

OM, SO_4^{2-}, NO_3^-, NH_4^+, EC, sea salt, mineral, TEO, K^+ contributed 13.98%, 18.03%, 10.23%, 7.78%, 3.61%, 3.4%, 8.4%, 1.08% and 1.44% of $PM_{2.5}$ mass, respectively, with apparent seasonal variation. As displayed in Fig. S3, spring was possessed of the highest contribution of sea salt and mineral in the four seasons, which was in good agreement with the seasonal tendency of Na^+ and Ca^{2+} caused by the great mechanical disruption of the ocean surface and the prevalence of dust events in spring. The highest contribution of SIA and TEO were found in summer. This can be ascribed to the perfect condition, such as opulent sunshine and oxidant, for the photochemistry and oxidation reaction at that point. Similar phenomenon was also reported in Beijing (Zhang et al. 2013). The proportions of OM, EC and K^+ were maximal in winter led by the great contribution of biomass burning and resident coal combustion as discussed above. Overall, SO_4^{2-}, NO_3^- and NH_4^+ maintained the major components in $PM_{2.5}$ throughout the year albeit with seasonal variation.

3.2.2. PMF model

By employing USEPA PMF5.0 model together with the obtained data set (120 samples × 28 species), source contribution of $PM_{2.5}$ was quantitatively explored. After iterative testing from 4 to 10 factors in modelling exercises, the pattern of seven factors were found providing the most physically reasonable source profiles with an F_{peak} value of −0.1 and the lowest Q value (7338). The identified factors were coal combustion + biomass burning, industry source, ship emission, sea salt, mineral dust, refined chrome industry and vehicle emission, respectively. Their source profiles and percentage contributions were shown in Fig. 6. The first factor interpreted high proportions of OC, EC, SO_4^{2-} and K^+, which matched a mixing emission profiles including coal combustion and biomass burning (Zhang et al. 2013). Generally, K^+ is an excellent tracer of biomass burning (Fourtziou et al. 2017), while coal combustion is often indicated by high OC, EC and SO_4^{2-} (Zong et al. 2016b). This factor was the largest contributor to SO_4^{2-}, consisting with its emission inventory in North China (Zhao et al. 2013; Liu et al. 2014). Fig. 6 also displayed the time series of daily contribution from each factors. It can be seen that higher contribution of this factor occurred in winter, indicating the dominant status of residential coal and biomass burning at coal time in North China

Table 1
Seasonal EFs for Co, Mn, Cr, V, Ni, Cu, As, Zn, Pb and Cd. The bold refers to the highest value.

	EF(V)	EF(Cr)	EF(Mn)	EF(Co)	EF(Ni)	EF(Cu)	EF(Zn)	EF(As)	EF(Cd)	EF(Pb)
Spring	121.18	**123.00**	20.13	17.12	250.13	218.44	675.41	217.72	4496.33	965.22
Summer	**188.32**	81.38	15.54	**17.77**	**330.79**	**391.86**	675.98	372.08	4644.47	1004.00
Autumn	97.21	102.38	24.22	15.32	225.62	307.02	**917.02**	308.67	5230.10	1418.44
Winter	55.02	78.51	**24.46**	16.00	148.85	381.28	769.50	**403.46**	**7186.47**	**2033.75**

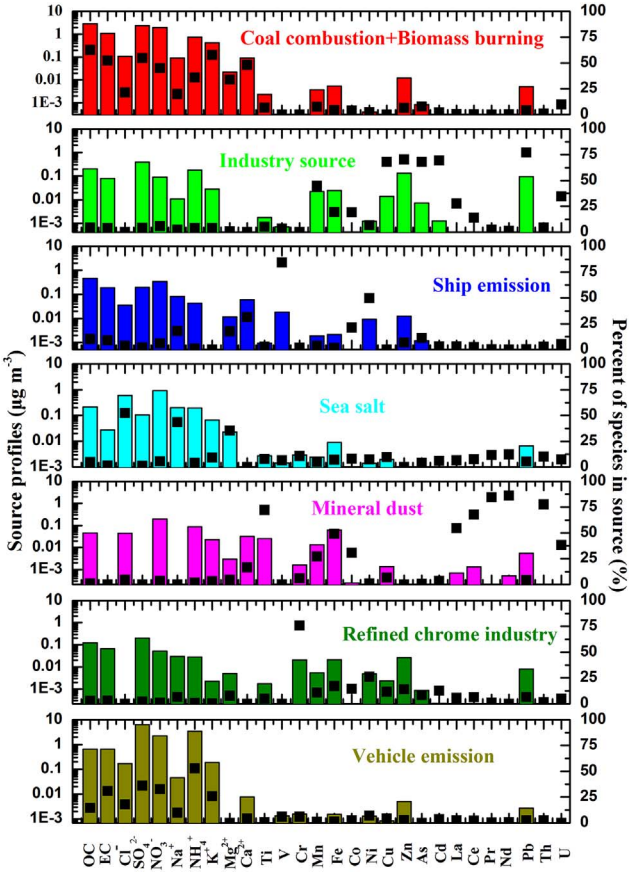

Fig. 6. Seven source profiles (bars) and percentage contributions (dots); time series of daily contribution from each identified source (continuous line).

(Fourtziou et al. 2017; Zhou et al. 2017). This agreed with the discussed above, such as the higher OC/EC ratio, M-K test result and the relative higher concentration of K^+ in winter.

The second factor was industry source, characterized by high Cu, Zn, As, Cd and Pb loadings. The factor profile was in line with that of Qimu Island in our previous study (Zong et al. 2016b). Equally, iron and steel industry may be very important among these industrial processes, because sintering process for iron and steel industry could produce a mass of heavy metals, especially for Cu, Pb and Zn (Y Wang et al. 2016c). In addition, the scale of steel production in North China was huge. As national statistical data shown, about half the world's production of crude steel was from China, while BTH region and Shandong province contributed 25.3% and 7.8%, respectively (http://www.stats.gov.cn/tjsj/ndsj/). Fig. 6 suggested industry source had higher contribution in winter, when the air masses mostly passed through the two regions (Fig. S1). The third factor represented ship emission characterized by high contributions of Ni and V and a high V/Ni ratio. High loadings of Ni and V are typically related with emissions of residual oil derived from ship activities (Pey et al. 2013). Previous study showed a high V/Ni ratio, usually > 0.7, is always considered as a symbol of aerosols influenced by ship emissions (Zhang et al. 2014). In this profile, the V/Ni ratio was 1.69. Meanwhile, higher contribution of this factor happened in summer (Fig. 6) corresponding with the fact that summer was the most frequent period of shipping in Bohai Sea due to the perfect conditions of weather and sea state (Wang et al. 2013), which was also in accordance with the EFs result.

The fourth factor was characterized by high loadings of Cl^-, Na^+ and Mg^{2+}, which was treated as signals of sea salt (Manousakas et al. 2017). It mostly came from the mechanical disruption of the sea surface. For example, winter and spring exhibited a relative higher contribution of this factor, and its highest contribution occurred at 28th April, 2015, when a strong wind raged in Bohai Sea. The Cl^-/Na^+ ratio was 1.43 in this profile, which was lower than the corresponding ratio in average seawater (1.80). This can be attributed to the Cl^- depletion as mentioned above (Masiol et al. 2017). The fifth factor was assigned as mineral dust with some typical crustal elements, such as Ti, Mn, Fe and rare earth metals (Xiong et al. 2017). The contribution of this factor was obvious higher in spring agreeing well with the prevalence of dust event at that time. The sixth factor, refined chrome industry, was characterized by high loading of Cr accompanied with some related metal elements (Mn, Fe, Co, Cu and Zn). Cr is one of the most important alloying elements. In China, Cr industry mainly distributes in Northeast China represented by some big chrome alloy factories, such as Jilin, Liaoyang, and Jinzhou. Correspondingly, summer demonstrated higher contribution for this factor, when part of air masses encountering BH Island derived from Northeast China (Fig. S1). Noticeably, this type of backward trajectory was significant different from other seasons. The seventh factors revealed high proportions of EC, NO_3^- and NH_4^+, which were all enriched in vehicle emission (Cui et al. 2016). Thereinto, NH_4^+ was from vehicles equipped with three-way catalytic converters with the rapid increase of the vehicle number in nowadays. In addition, Fig. 6 indicated this factor's contribution held no obvious seasonal variation, manifesting vehicle pollution in North China having regional feature.

Fig. 7 describes the respective contribution of the seven factors to $PM_{2.5}$. Obviously, coal combustion + biomass burning and vehicle emission were the dominant contributors, accounting for 48.21% and 30.33%, respectively, during the study period. They were followed by mineral dust (7.24%), ship emission (6.63%), sea salt (3.51%), industry source (3.2%) and refined chrome industry (0.88%) in the decreasing order. Comparatively, this PMF result was basically equal to that of chemical mass closure, validating the effectiveness of modelling simulation. For example, the contribution of sea salt was 3.51% in PMF result, and that in chemical mass closure was 3.4%. While the contribution of mineral dust was relative lower in PMF result, which may be caused by the irrelevant classification.

3.3. Regional source deduced from PSCF analysis

Based on the described above, we can see that the regional sources and transports of $PM_{2.5}$ could exert a significant influence on the air quality of BH Island. To get a better understanding of this issue, the PSCF analysis on account of HYSPLIT model was used for identifying the potential source regions of the seven source factors given by PMF result (Bressi et al. 2014). Fig. 8 shows the PSCF map produced using the daily contribution date with the 75th percentile cut of each source factor. The colours represent the contribution level of regions, and dark colour could be associated with the high possibility for the grid cell to be an emission source, while the light colour indicated low possibility. Based on this map, the region surrounding Shandong peninsula and Hebei province were identified as the mediums to high potential region for coal combustion + biomass burning in North China, which was consistent with that found by previous studies. For example, Zong et al.

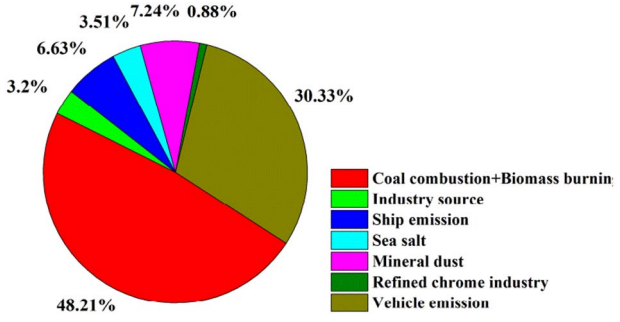

Fig. 7. The respective contribution of the seven factors to $PM_{2.5}$ on BH Island.

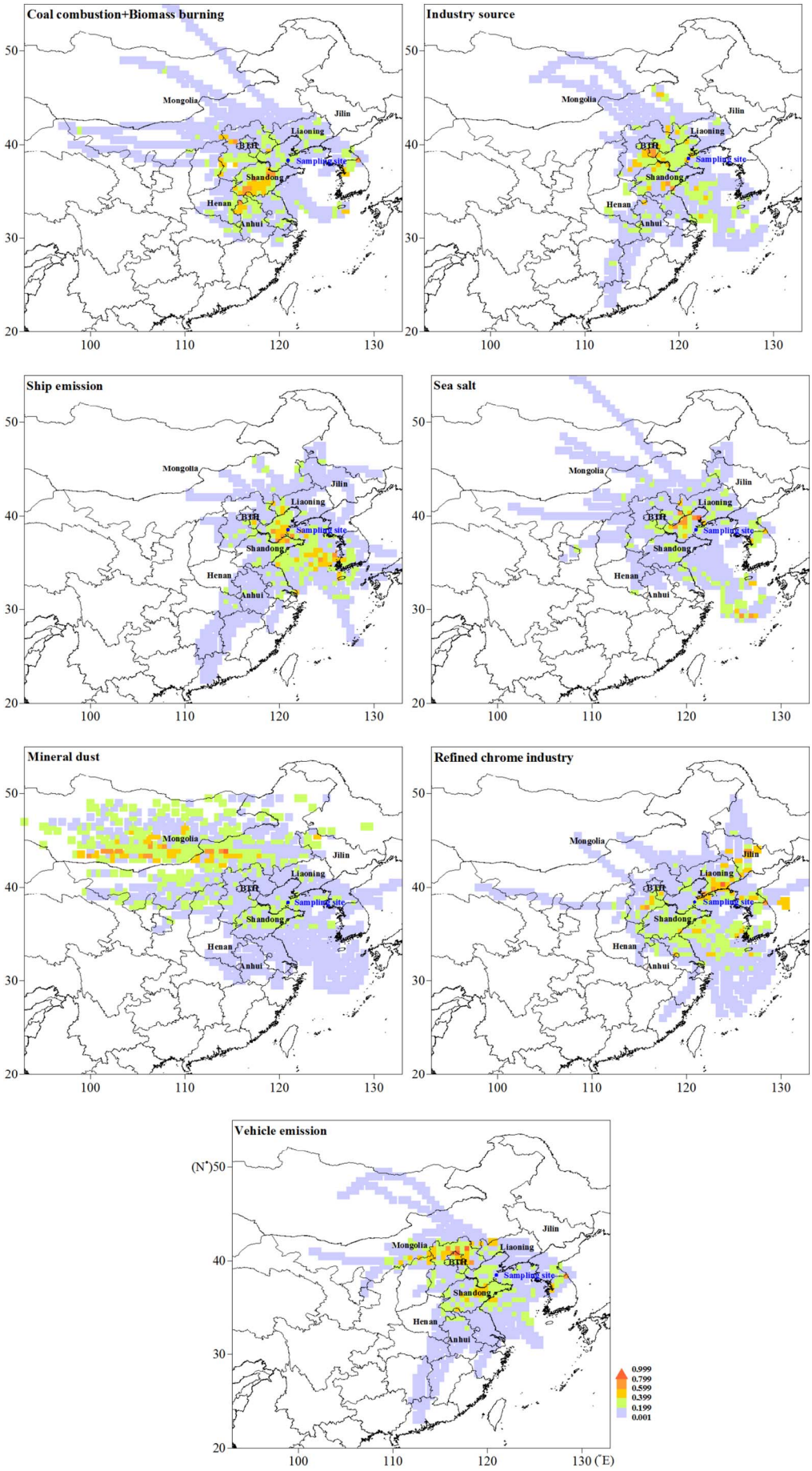

Fig. 8. The PSCF maps of coal combustion + biomass burning, industry source, ship emission, sea salt, mineral dust, refined chrome industry and vehicle emission.

(Zong et al. 2016b) suggested biomass burning from Shandong peninsula contributed a large portion of $PM_{2.5}$ in North China. In addition, it was noted that high contribution of this mixed source frequently occurred in cool season, when most back trajectories passed through the two regions. There were a large number of grid cells with PSCF values > 0.6 from the BTH region for industry source, indicating this region was an important industry seminary for $PM_{2.5}$ in North China (Yao et al. 2016). It also agreed with mentioned above, illustratively, the contribution of crude steel in BTH region could occupy about 25.3% in China, which contributed half of the world's production of crude steel. Bohai Sea and East China Sea were found to be of high source potential for ship emission (Zhang et al. 2014), where a great number of ships were running. As reported, 0.18 million water transport vessels and 1.07 million fishing boats active in Chinese sea by 2013, of which 1/3 lay in Bohai Sea. Besides, ship activities distributing in west coast of Korea may also influence this source (Song and Shon 2014).

Regarding sea salt, the high probability partly came from geographical regions located northwest of BH Island. The mechanical disruption of sea surface was the dominant source for sea salt, which significantly hung on the high wind speed. Impacted by the East winter monsoon, the strong northwest wind became the source causer for BH Island. In addition, East China Sea affected by summer storms was also important source region. Mineral dust presumably came from the region of Mongolia. In fact, plenty of studies have suggested that Mongolia could be the main source region of dust emission for North China. When comparing mineral dust and refined chrome industry, distinct feature from the map can be found. Refined chrome industry mostly came from Liaoning, Jilin province and a lesser extent from BTH region and Shandong peninsula although contribution from overseas was also relative noticeable. This distribution area was consistent with the locations of some big chrome alloy factories, such as Jilin, Liaoyang, Jinzhou and Shougang as mentioned above. Lastly, vehicle emission was primarily of BTH region origin, centred on metropolises, such as Beijing and Tianjin. Indeed, vehicle emission is becoming one of the most important sources of severe air pollution due to the huge quantity and sharp growth of vehicles in Chinese megacities (Guo et al. 2016). Moreover, Shandong peninsula was also identified as an important source region, as except for the acknowledged high level of vehicle emission in BTH region, there were also many vehicle sources existing in Shandong peninsula. For example, the car ownership in Shandong province has ranked first in China by 2013 (Zong et al. 2016a).

4. Conclusions

The annual average concentration of $PM_{2.5}$ was 63.10 ± 39.00 μg m^{-3} on BH Island, a regional background site in North China. Compared with other regions in China, it was notably lower than typical urban areas, while was similar with some background sites, indicating our measurement primarily reflected a regional pollution pattern. A distinct seasonal variation of $PM_{2.5}$ was observed with the highest concentration in winter and the lowest value in summer. The average concentration of OC and EC was 4.90 ± 3.69 and 2.28 ± 1.69 μg m^{-3} accounting for 7.77% and 3.61% of $PM_{2.5}$, respectively. The consistent variation and good relationship between OC and EC suggested their strong co-emission during the sampling period. Biomass burning and residential coal combustion may be important sources for OC and EC in winter based on the higher OC/EC ratio and M-K test result. Among WSI, SO_4^{2-} ranked the highest with a mean concentration of 11.38 ± 10.26 μg m^{-3}, followed by NO_3^-, NH_4^+, Cl^-, K^+, Na^+, Ca^{2+} and Mg^{2+}. In the thermodynamic equilibrium condition, SO_4^{2-} and NO_3^- were mostly combined with NH_4^+ presenting in the form of NH_4NO_3 and $(NH4)_2SO_4$, while the remainder SO_4^{2-} neutralized the alkalis, all Cl^- was exclusively presented in the form of NH_4Cl. Total concentration of analyzed inorganic elements was 781.82 ± 670.96 ng m^{-3}, which accounted for 1.24% of the $PM_{2.5}$ mass. The EFs analysis implied Cr, V, Ni, Cu, Zn, As, Cd and Pb originated predominantly from human activities.

Chemical mass closure of $PM_{2.5}$ was successfully conducted on an annual and seasonal basis. Results showed that OM, SO_4^{2-}, NO_3^-, NH_4^+, EC, sea salt, mineral, TEO, K^+ contributed 13.98%, 18.03%, 10.23%, 7.78%, 3.61%, 3.4%, 8.4%, 1.08% and 1.44% of $PM_{2.5}$ mass, respectively, with apparent seasonal variation. Based on PMF model, seven source factors were identified; they are coal combustion + biomass burning (48.21%), vehicle emission (30.33%), mineral dust (7.24%), ship emission (6.63%), sea salt (3.51%), industry source (3.2%) and refined chrome industry (0.88%), respectively. Comparatively, this PMF result was basically equal to that of chemical mass closure, validating the effectiveness of modelling result. In addition, PSCF analysis using the daily contribution of each factor from PMF result was adopted to identify their potential source regions. Shandong peninsula and Hebei province were identified as high potential regions for coal combustion + biomass burning; BTH region was the main source region for industry source; Bohai Sea and East China Sea were found to be of high source potential for ship emission; Geographical regions located northwest of BH Island was possessed of high probability for sea salt; Mineral dust presumably came from the region of Mongolia; Refined chrome industry mostly came from Liaoning, Jilin province and a lesser extent from BTH region; The vehicle emission was primarily of BTH region origin, centred on metropolises, such as Beijing and Tianjin. Considering their respective contribution in $PM_{2.5}$, coal combustion + biomass burning in Shandong peninsula and Hebei province, and vehicle emission in BTH should be critically managed for the $PM_{2.5}$ alleviation in North China.

Acknowledgements

This work was supported by the CAS Strategic Priority Research Program (Nos. XDA11020402, XDB05030303), and the Natural Scientific Foundation of China (Nos. 41471413; 31370464). The authors gratefully acknowledge the National Oceanic and Atmospheric Administration's Air Resources Laboratory for providing the HYSPLIT transport model and the READY website (http://www.arl.noaa.gov/ready.html). The authors also acknowledge the office-holders of Environmental Monitoring Station of State Ocean Administration of China on Beihuangcheng (BH) Island for the sampling work.

Appendix A. Supplementary data

Supplementary data to this article can be found online at https://doi.org/10.1016/j.atmosres.2017.12.013.

References

Amil, N., Latif, M.T., Khan, M.F., Mohamad, M., 2016. Seasonal variability of $PM_{2.5}$ composition and sources in the Klang Valley urban-industrial environment. Atmos. Chem. Phys. 16, 5357–5381.

Bressi, M., Sciare, J., Ghersi, V., Mihalopoulos, N., Petit, J.E., Nicolas, J.B., et al., 2014. Sources and geographical origins of fine aerosols in Paris (France). Atmos. Chem. Phys. 14, 8813–8839.

Cui, M., Chen, Y., Tian, C., Zhang, F., Yan, C., Zheng, M., 2016. Chemical composition of $PM_{2.5}$ from two tunnels with different vehicular fleet characteristics. Sci. Total Environ. 550, 123–132.

Du, Z., He, K., Cheng, Y., Duan, F., Ma, Y., Liu, J., et al., 2014. A yearlong study of water-soluble organic carbon in Beijing I: sources and its primary vs. secondary nature. Atmos. Environ. 92, 514–521.

Feng, Y., Chen, Y., Guo, H., Zhi, G., Xiong, S., Li, J., et al., 2009. Characteristics of organic and elemental carbon in $PM_{2.5}$ samples in shanghai, China. Atmos. Res. 92, 434–442.

Fourtziou, L., Liakakou, E., Stavroulas, I., Theodosi, C., Zarmpas, P., Psiloglou, B., et al., 2017. Multi-tracer approach to characterize domestic wood burning in Athens (Greece) during wintertime. Atmos. Environ. 148, 89–101.

Genga, A., Ielpo, P., Siciliano, T., Siciliano, M., 2017. Carbonaceous particles and aerosol mass closure in $PM_{2.5}$ collected in a port city. Atmos. Res. 183, 245–254.

Gibson, M.D., Pierce, J.R., Waugh, D., Kuchta, J.S., Chisholm, L., Duck, T.J., et al., 2013. Identifying the sources driving observed $PM_{2.5}$ temporal variability over Halifax, Nova Scotia, during BORTAS-B. Atmos. Chem. Phys. 13, 7199–7213.

Guo, X., Fu, L., Ji, M., Lang, J., Chen, D., Cheng, S., 2016. Scenario analysis to vehicular emission reduction in Beijing-Tianjin-Hebei (BTH) region, China. Environ. Pollut. 216, 470–479.

Hu, G., Zhang, Y., Sun, J., Zhang, L., Shen, X., Lin, W., et al., 2014. Variability, formation and acidity of water-soluble ions in $PM_{2.5}$ in Beijing based on the semi-continuous

observations. Atmos. Res. 145-146, 1–11.
Huang, K., Zhuang, G., Li, J., Wang, Q., Sun, Y., Lin, Y., et al., 2010. Mixing of Asian dust with pollution aerosol and the transformation of aerosol components during the dust storm over China in spring 2007. J. Geophys. Res.-Atmos. 115.
Huang, D., Xiu, G., Li, M., Hua, X., Long, Y., 2017. Surface components of $PM_{2.5}$ during clear and hazy days in Shanghai by ToF-SIMS. Atmos. Environ. 148, 175–181.
Kotchenruther, R.A., 2016. Source apportionment of $PM_{2.5}$ at multiple northwest US sites: assessing regional winter wood smoke impacts from residential wood combustion. Atmos. Environ. 142, 210–219.
Kumar, M., Raju, M.P., Singh, R.K., Singh, A.K., Singh, R.S., Banerjee, T., 2017. Wintertime characteristics of aerosols over middle Indo-Gangetic plain: vertical profile, transport and radiative forcing. Atmos. Res. 183, 268–282.
Lewandowski, M., Jaoui, M., Kleindienst, T.E., Offenberg, J.H., Edney, E.O., 2007. Composition of $PM_{2.5}$ during the summer of 2003 in Research Triangle Park, North Carolina. Atmos. Environ. 41, 4073–4083.
Li, H., Wang, Q.G., Yang, M., Li, F., Wang, J., Sun, Y., et al., 2016. Chemical characterization and source apportionment of $PM_{2.5}$ aerosols in a megacity of Southeast China. Atmos. Res. 181, 288–299.
Liu, D., Li, J., Zhang, Y., Xu, Y., Liu, X., Ding, P., et al., 2013. The use of levoglucosan and radiocarbon for source apportionment of $PM_{2.5}$ carbonaceous aerosols at a background site in East China. Environ. Sci. Technol. 47, 10454–10461.
Liu, J., Li, J., Zhang, Y., Liu, D., Ding, P., Shen, C., et al., 2014. Source apportionment using radiocarbon and organic tracers for $PM_{2.5}$ carbonaceous aerosols in Guangzhou, South China: contrasting local- and regional-scale haze events. Environ. Sci. Technol. 48, 12002–12011.
Manousakas, M., Papaefthymiou, H., Diapouli, E., Migliori, A., Karydas, A.G., Bogdanovic-Radovic, I., et al., 2017. Assessment of $PM_{2.5}$ sources and their corresponding level of uncertainty in a coastal urban area using EPA PMF 5.0 enhanced diagnostics. Sci. Total Environ. 574, 155–164.
Masiol, M., Hopke, P.K., Felton, H.D., Frank, B.P., Rattigan, O.V., Wurth, M.J., et al., 2017. Source apportionment of $PM_{2.5}$ chemically speciated mass and particle number concentrations in New York City. Atmos. Environ. 148, 215–229.
Niu, X., Cao, J., Shen, Z., Ho, S.S.H., Tie, X., Zhao, S., et al., 2016. $PM_{2.5}$ from the Guanzhong plain: chemical composition and implications for emission reductions. Atmos. Environ. 147, 458–469.
Pan, Y., Wang, Y., Zhang, J., Liu, Z., Wang, L., Tian, S., et al., 2016. Redefining the importance of nitrate during haze pollution to help optimize an emission control strategy. Atmos. Environ. 141, 197–202.
Perrino, C., Catrambone, M., Farao, C., Canepari, S., 2016. Assessing the contribution of water to the mass closure of PM_{10}. Atmos. Environ. 140, 555–564.
Pey, J., Perez, N., Cortes, J., Alastuey, A., Querol, X., 2013. Chemical fingerprint and impact of shipping emissions over a western Mediterranean metropolis: primary and aged contributions. Sci. Total Environ. 463, 497–507.
Shahsavani, A., Naddafi, K., Haghighifard, N.J., Mesdaghinia, A., Yunesian, M., Nabizadeh, R., et al., 2012. Characterization of ionic composition of TSP and PM_{10} during the middle eastern dust (MED) storms in Ahvaz, Iran. Environ. Monit. Assess. 184, 6683–6692.
Song, S.-K., Shon, Z.-H., 2014. Current and future emission estimates of exhaust gases and particles from shipping at the largest port in Korea. Environ. Sci. Pollut. Res. 21, 6612–6622.
Tan, J.H., Duan, J.C., Ma, Y.L., Yang, F.M., Cheng, Y., He, K.B., et al., 2014. Source of atmospheric heavy metals in winter in Foshan, China. Sci. Total Environ. 493, 262–270.
Tao, J., Gao, J., Zhang, L., Zhang, R., Che, H., Zhang, Z., et al., 2014. $PM_{2.5}$ pollution in a megacity of southwest China: source apportionment and implication. Atmos. Chem. Phys. 14, 8679–8699.
Tian, M., Wang, H., Chen, Y., Yang, F., Zhang, X., Zou, Q., et al., 2016. Characteristics of aerosol pollution during heavy haze events in Suzhou, China. Atmos. Chem. Phys. 16, 7357–7371.
Wang, X., Bi, X., Sheng, G., Hospital, Fu H., 2006. Indoor $PM_{10}/PM_{2.5}$ and associated trace elements in Guangzhou, China. Sci. Total Environ. 366, 124–135.
Wang, L., Qi, J.H., Shi, J.H., Chen, X.J., Gao, H.W., 2013. Source apportionment of particulate pollutants in the atmosphere over the northern Yellow Sea. Atmos. Environ. 70, 425–434.
Wang, X., Chen, Y., Tian, C., Huang, G., Fang, Y., Zhang, F., et al., 2014. Impact of agricultural waste burning in the Shandong peninsula on carbonaceous aerosols in the Bohai Rim, China. Sci. Total Environ. 481, 311–316.
Wang, G., Zhang, R., Gomez, M.E., Yang, L., Zamora, M.L., Hu, M., et al., 2016. Persistent sulfate formation from London fog to Chinese haze. Proc. Natl. Acad. Sci. U. S. A. 113, 13630–13635.
Wang, S.-H., Hung, W.-T., Chang, S.-C., Yen, M.-C., 2016. Transport characteristics of Chinese haze over northern Taiwan in winter, 2005–2014. Atmos. Environ. 126, 76–86.
Wang, Y., Jia, C., Tao, J., Zhang, L., Liang, X., Ma, J., et al., 2016. Chemical characterization and source apportionment of $PM_{2.5}$ in a semi-arid and petrochemical-industrialized city, Northwest China. Sci. Total Environ. 573, 1031–1040.
Wu, H., Zhang, Y.-F., Han, S.-Q., Wu, J.-H., Bi, X.-H., Shi, G.-L., et al., 2015. Vertical characteristics of $PM_{2.5}$ during the heating season in Tianjin, China. Sci. Total Environ. 523, 152–160.
Xiong, Y., Zhou, J., Schauer, J.J., Yu, W., Hu, Y., 2017. Seasonal and spatial differences in source contributions to $PM_{2.5}$ in Wuhan, China. Sci. Total Environ. 577, 155–165.
Yang, F., Tan, J., Zhao, Q., Du, Z., He, K., Ma, Y., et al., 2011. Characteristics of $PM_{2.5}$ speciation in representative megacities and across China. Atmos. Chem. Phys. 11, 5207–5219.
Yao, L., Yang, L., Yuan, Q., Yan, C., Dong, C., Meng, C., et al., 2016. Sources apportionment of $PM_{2.5}$ in a background site in the North China plain. Sci. Total Environ. 541, 590–598.
Zhang, R., Jing, J., Tao, J., Hsu, S.C., Wang, G., Cao, J., et al., 2013. Chemical characterization and source apportionment of $PM_{2.5}$ in Beijing: seasonal perspective. Atmos. Chem. Phys. 13, 7053–7074.
Zhang, F., Chen, Y., Tian, C., Wang, X., Huang, G., Fang, Y., et al., 2014. Identification and quantification of shipping emissions in Bohai Rim, China. Sci. Total Environ. 497-498, 570–577.
Zhao, B., Wang, P., Ma, J.Z., Zhu, S., Pozzer, A., Li, W., 2012. A high-resolution emission inventory of primary pollutants for the Huabei region, China. Atmos. Chem. Phys. 12, 481–501.
Zhao, P.S., Dong, F., He, D., Zhao, X.J., Zhang, X.L., Zhang, W.Z., et al., 2013. Characteristics of concentrations and chemical compositions for $PM_{2.5}$ in the region of Beijing, Tianjin, and Hebei, China. Atmos. Chem. Phys. 13, 4631–4644.
Zhou, S., Yang, L., Gao, R., Wang, X., Gao, X., Nie, W., et al., 2017. A comparison study of carbonaceous aerosols in a typical North China plain urban atmosphere: seasonal variability, sources and implications to haze formation. Atmos. Environ. 149, 95–103.
Zong, Z., Chen, Y., Tian, C., Fang, Y., Wang, X., Huang, G., et al., 2015. Radiocarbon-based impact assessment of open biomass burning on regional carbonaceous aerosols in North China. Sci. Total Environ. 518-519, 1–7.
Zong, Z., Wang, X., Tian, C., Chen, Y., Han, G., Li, J., et al., 2016a. Source and formation characteristics of water-soluble organic carbon in the anthropogenic-influenced Yellow River Delta, North China. Atmos. Environ. 144, 124–132.
Zong, Z., Wang, X., Tian, C., Chen, Y., Qu, L., Ji, L., et al., 2016b. Source apportionment of $PM_{2.5}$ at a regional background site in North China using PMF linked with radiocarbon analysis: insight into the contribution of biomass burning. Atmos. Chem. Phys. 16, 11249–11265.